Comparative Performance Evaluation of Lorentz Torque and Conventional Damping Techniques for Wind Turbine Blade Vibration Control Using MATLAB/Simulink

Aliyu Abubakar [1] Mutari Hajara Ali[2]
[1] Department of Electrical and Electronics Engineering, Federal Polytechnic, Bali. Taraba State.
[2] Department of Physics, College of Natural and pharmaceutical sciences, Faculty of Physical Sciences, Bayero University, Kano, Nigeria
[1]babandubu@gmail.com

ABSTRACT

This paper presents a unified MATLAB/Simulink-based comparative evaluation of a Lorentz torque damper and nine conventional passive, semi-active, and active damping techniques for wind turbine blade vibration control. All damping systems are implemented on an identical blade–generator dynamic model and subjected to the same gust-induced aerodynamic excitation to ensure objective comparison. Performance is assessed using settling time, root mean square (RMS) vibration amplitude, overshoot, added structural mass, energy consumption, maintenance demand index, vibration suppression efficiency, and cost index. Simulation results show that the Lorentz torque damper achieves the shortest settling time (3.25–5.01 s), the lowest RMS vibration amplitude (62–71% reduction), minimal overshoot, negligible added mass, and the lowest energy and maintenance requirements among all evaluated techniques. These findings demonstrate that Lorentz torque damping provides a lightweight, energy-efficient, and economically viable solution for large-scale wind turbine blade vibration mitigation.
Keywords: Electromagnetic damping; Lorentz torque damper; MATLAB/Simulink; Settling time; Vibration control; Wind turbine blades.

1 INTRODUCTION

Wind energy continues to expand rapidly due to global decarbonization targets, technological advancements, and declining installation costs (Li *et al*., 2020). However, wind turbines operate under highly stochastic atmospheric conditions, including turbulence, gusts, wind shear, and tower shadow effects, which induce unsteady aerodynamic loading and excite structural vibrations, particularly in flexible rotor blades (Panagiotis, 2024).

Wind turbine blades experience continuous cyclic loading throughout their service life. Excessive vibration accelerates fatigue damage, increases acoustic emissions, reduces aerodynamic efficiency, and shortens component lifespan, thereby increasing maintenance costs and reducing turbine availability (Kavade *et al.*, 2024). Effective vibration mitigation is therefore a critical requirement for reliable and cost-effective wind turbine operation (Zhang *et al*., 2024).

Existing vibration mitigation approaches include passive systems (tuned mass dampers, tuned liquid dampers, hydraulic dampers, friction dampers, and rotational inertia dampers) and active or semi-active systems (piezoelectric, electromagnetic, active mass driver, and active hydraulic dampers) (Machado & Dutkiewicz, 2024). Passive systems are simple and inherently stable but

[1] Corresponding Author: babandubu@gmail.com

often introduce significant added mass and are sensitive to tuning (Sumair *et al*., 2021). Active systems provide superior control authority but suffer from high energy consumption, increased system complexity, and elevated maintenance demands (Gönül et al., 2021).

Although numerous studies have investigated individual damping technologies, no prior work has provided a unified, multi-metric comparative assessment of passive, semi-active, and active damping techniques against a Lorentz torque damper using identical modeling assumptions, excitation profiles, and tuning criteria. Furthermore, critical trade-offs among vibration suppression capability, added mass, energy consumption, maintenance demand, and economic cost are rarely quantified simultaneously.

This study addresses these gaps by presenting a systematic, simulation-based comparative evaluation of a Lorentz torque damper and nine conventional damping techniques within a consistent MATLAB/Simulink framework.

2. SYSTEM MODELING AND DAMPING FRAMEWORK

A coupled wind turbine blade–generator system is modeled as a second-order rotational dynamic system to facilitate consistent time- and frequency-domain analysis (Machado & Dutkiewicz, 2024). All damping techniques are implemented within the same MATLAB/Simulink environment and subjected to identical excitation profiles (Chong *et al*., 2021). This unified modeling framework ensures objectivity and comparability across all evaluated damping strategies.

2.1 Wind Turbine Blade Dynamics

The wind turbine blade is modeled as a second-order rotational dynamic system subjected to aerodynamic, gust-induced, and control torques:. The wind turbine blade–generator system is modeled as a second-order rotational dynamic system .*(Bin et al.,* 2018*)*

$$J_b\ddot{\theta} + B_b\dot{\theta} + k_b\theta = T_{wind} + T_{gust} - T_{control} \quad (2.1)$$

Table 1 summarizes the key blade dynamic parameters employed in the analysis.

Parameter	Description	Unit
Jb	Blade rotational inertia	kg·m²
Bb	Structural damping coefficient	N·m·s/rad
Kb	Blade stiffness	N·m/rad
θ	Angular displacement	rad
Tw	Aerodynamic torque	N·m
Tg	Gust-induced torque	N·m
Tcontrol	Damping torque	N·m

The corresponding transfer function describes the blade's response to external excitation in the frequency domain and forms the basis for comparative damping analysis.

From this, the system can be converted to the frequency domain to describe how the blade responds to external torques at different frequencies. The resulting transfer function is given in Equation (Panagiotis, 2024).

$$\frac{\theta(s)}{T_{wind}+T_{gust}-T_{control}} = \frac{1}{J_b s^2+c_b s+k_b} \quad (2.2)$$

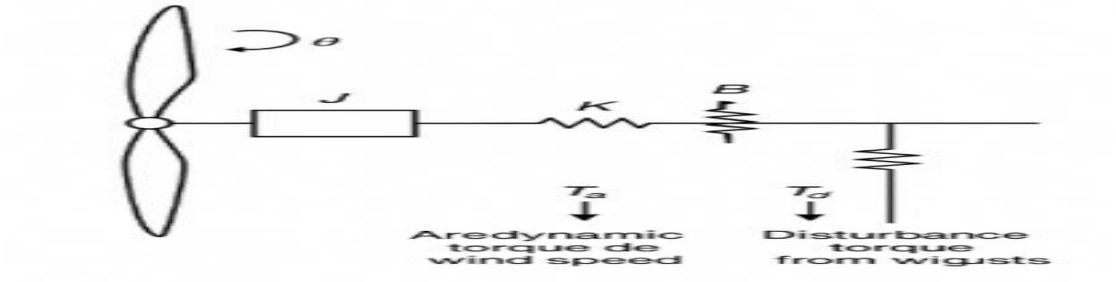

Figure 2.1 illustrates the wind turbine blade dynamic model used in this study (Meng & Sun, 2017).

Schematic representation of a wind turbine blade modeled as a second-order rotational system with inertia, damping, stiffness, and applied aerodynamic, gust, and control torques.

2.2 GENERATOR TORQUE DYNAMICS

Generator dynamics are modeled to capture the interaction between mechanical blade motion and electromagnetic torque. The generator's inertia and viscous damping influence the coupled blade–shaft response, enabling realistic simulation of electromechanical vibration behavior. The generator torque balance is expressed as: (Machado & Dutkiewicz, 2024)

$$J\ddot{\theta} = T_m - T_e - B\dot{\theta} \quad (2.3)$$

where J is the Generator rotational inertia (kg·m²), $T_m is\ the$ Mechanical torque from wind (N·m), $T_e\ is\ the$ Electrical torque produced by the generator (N·m) B is the Generator viscous friction coefficient (N·m·s/rad), θ is the Generator shaft angular displacement (rad)

The corresponding transfer function is (Kocabiyikoğlu, 2020):

$$\frac{\theta(s)}{T_m-T_e} = \frac{1}{Js^2+Bs} \quad (2.4)$$

where s is the complex root, J is inertia, B is the damping coefficient, $T_m and\ T_e$ are mechanical and electrical torques respectively

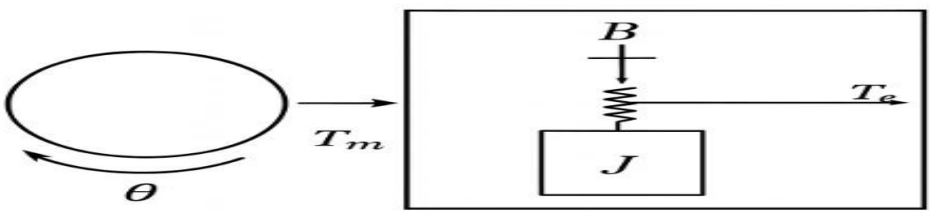

Figure 2.7.2 presents the generator dynamic model used in the simulations (Huang *et al*., 2021).

Diagram illustrating generator inertia, viscous damping, mechanical torque input, and electrical torque output.

2.3 DAMPING SYSTEMS OVERVIEW

Nine conventional damping techniques and the Lorentz torque damper are implemented on a common blade–generator model, where conventional dampers depend on added mass, fluid dynamics, friction, or active control and are associated with inertia effects, response delays, or continuous power requirements, whereas the Lorentz torque damper employs velocity-dependent electromagnetic damping without mechanical contact, enabling fast, broadband vibration suppression with negligible added mass and low energy demand (Ismaiel, 2023).

2.3.1 Tuned Mass Damper (TMD)

A secondary mass in a spring–damper configuration absorbs vibrational energy from the primary blade system. Governing equations and transfer functions describe energy exchange between the blade and the auxiliary mass (Kim *et al*., 2015.).

$$J\ddot{\theta}_{TMD} + B\dot{\theta}_{TMD} + K\theta_{TMD} + c_t(\dot{\theta} - \dot{x}_t) + k_t(\theta - x_t) = T_{gust} \qquad (2.8)$$

and $$m_t\ddot{x}_t + c_t(\dot{x}_t - \dot{\theta}) + k_t(x_t - \theta) = 0 \qquad (2.9)$$

$$\frac{\boldsymbol{\theta(s)}}{\boldsymbol{T_{gust}}} = \frac{\boldsymbol{m_t}s^2 + c_t s + k_t}{(\mathbf{s^2 + Bs + K})(\boldsymbol{m_t}s^2 + c_t s + k_t) - (c_t s - k_t)^2} \qquad (\mathbf{2.10})$$

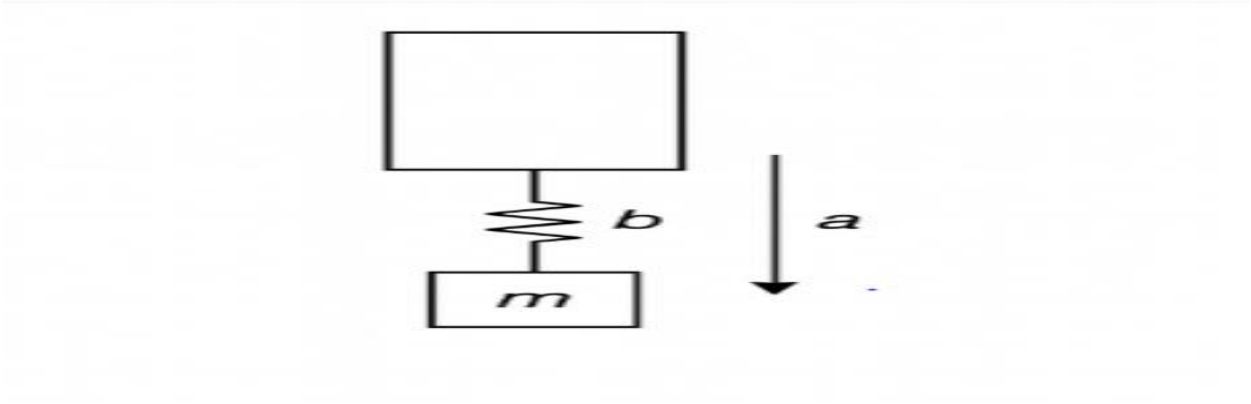

Figure 2.9.1: *Tuned Mass Damper (TMD) for Blade Vibration* (Engineering, 2021)

2.3.2 Active Frictional Clutch Damper

Friction plates provide controllable resistance to motion, reducing vibrations and enhancing stability. The system is characterized by torque–velocity relationships governing the damping effect (Wagner, 2017).

$$J\ddot{\theta}_b + (B_b + c_f)\dot{\theta}_b + K\theta_b = T_{gust} \quad (2.11)$$

The transfer function of the tuned liquid damper is expressed as follows:

$$\frac{\theta(s)}{T_{gust}(s)} = \frac{1}{Js^2 + (B_b + c_f)s + K_b} \quad (2.12)$$

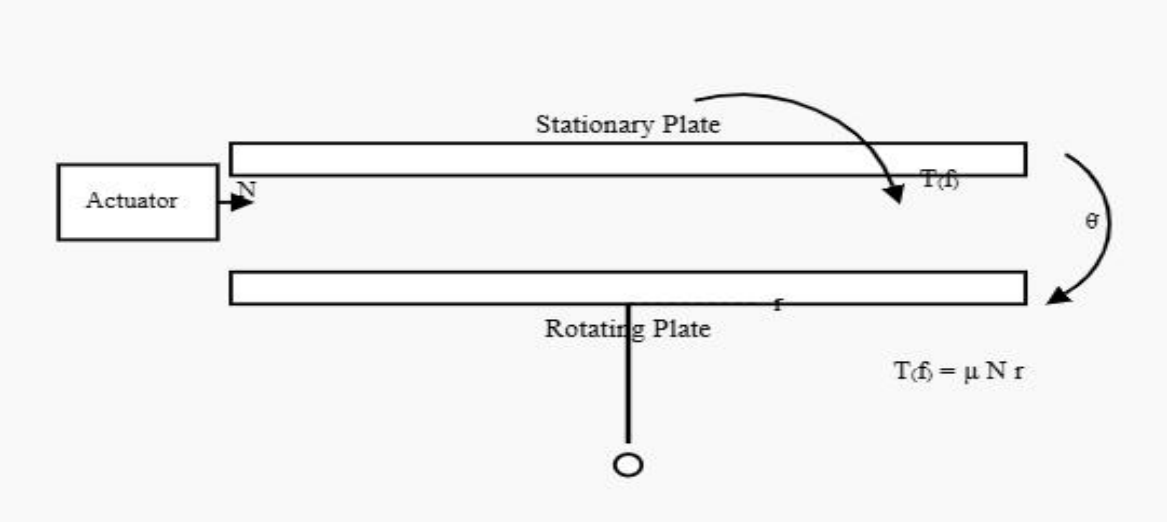

Figure 2.9.2: *Active Frictional Clutch Damper* (Qansh, 2022)

Diagram showing actuator-controlled friction plates producing nonlinear resisting torque proportional to blade velocity. Its frictional force is governed by:

2.3.3 Active Hydraulic Damper

Hydraulic fluid flow is modulated to counteract blade vibrations in real time. Transfer functions describe the interaction between fluid dynamics and blade motion (J. Li et al., 2024).

$$J\ddot{\theta} + (B_b + c_{AH})\dot{\theta}_{AH} + (K_b + K_{AH})\theta_{AH} = T_{gust} \quad (2.13)$$

The transfer function of an active hydraulic damper can be expressed as follows:

$$\frac{\theta(s)}{T_{gust}(s)} = \frac{1}{s^2 + (B_b + c_{AH})s + (K_b + K_{AH})} \quad (2.14)$$

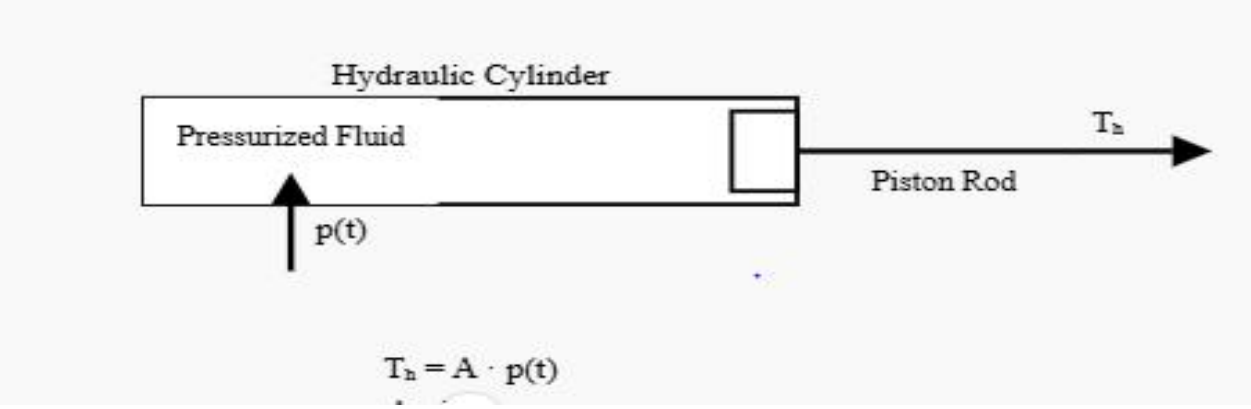

Figure 2.9.3: *Active Hydraulic Damper* (Awada *et al*., 2021)

Representation of a hydraulic chamber generating controllable torque via modulated fluid pressure.

2.3.4 Electromagnetic Damper

Motion of a conductor through a magnetic field generates eddy currents producing a resistive damping torque. This provides smooth, non-contact vibration control (Chen *et al*., 2023).

$$J\ddot{\theta}_L + (B + c_{ED})\dot{\theta}_L + K\theta = T_{gust} \qquad (2.15)$$

The transfer function of the electromagnetic damper is expressed as follows:

$$\frac{\theta(s)}{T_{gust}(s)} = \frac{1}{Js^2 + (B + c_{ED})s + K} \qquad (2.16)$$

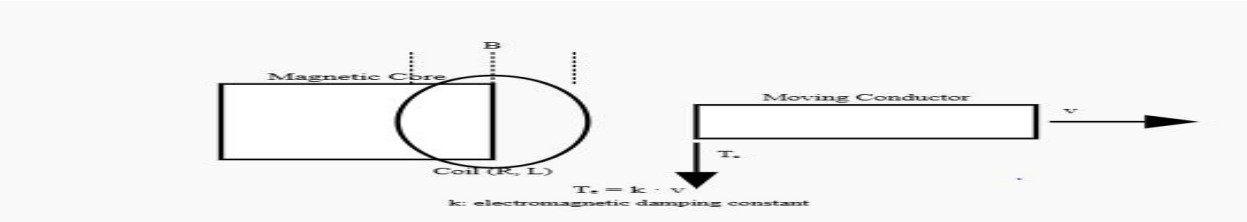

Figure 2.9.4: *Electromagnetic Damper* (Meng & Sun, 2017)

Schematic illustrating eddy-current or magnetic field-induced torque opposing blade motion.

2.3.5 Active Piezoelectric Damper

Piezoelectric materials generate counteracting forces in response to structural strain, mitigating vibrations. Governing equations link mechanical deformation to induced electrical forces (Huang et al., 2021).

$$J\ddot{\theta}_p + (B + c_p)\dot{\theta}_p + (K + K_p)\theta_p = T_{gust} \quad (2.17)$$

The transfer function of the tuned liquid damper is expressed as follows:

$$\frac{\theta(s)}{T_{gust}(s)} = \frac{1}{Js^2 + (B + c_p)s + (K + K_p)} \quad (2.18)$$

Figure 2.9.5: *Active Piezoelectric Damper* (Wang *et al*., 2025)

Diagram showing piezoelectric actuators converting electrical input into counteracting mechanical forces.

2.3.6 Rotational Inertia Damper

A spinning flywheel generates angular momentum to resist rapid rotational changes. This mechanical resistance smooths motion and suppresses blade vibrations(Kim *et al*., 2015.).

$$(J_b + J_f)\ddot{\theta}_b + B\dot{\theta}_b + K\theta = T_{gust} \quad (2.19)$$

By implementing a rotational inertia damper in mechanical systems, engineers can achieve improved stability, safety, and longevity of the equipment, ultimately leading to better performance and reduced maintenance requirements.

The transfer function of the rotational inertia damper is represented by the following expression:

$$\frac{\theta(s)}{T_{gust}(s)} = \frac{1}{(J_b + J_f)s^2 + B_b s + K_b} \quad (2.20)$$

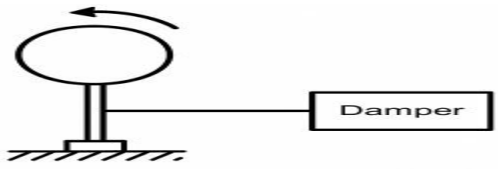

Figure 2.9.6: *Rotational Inertia Damper* (Wang et al., 2025)

Illustration of a flywheel attached to the blade or shaft, where angular momentum resists motion changes to suppress vibrations.

2.3.7 Active Mass Driver Damper

A motor-driven mass moves to counteract structural vibrations in real time. Sensor feedback and control laws govern the mass motion to reduce blade oscillations (Kim et al., 2015.).

$$J\ddot{\theta}_{AMD} + (B_b + c_{AMD})\dot{\theta}_L + (K_b + K_{AMD})\theta = T_{gust} \quad (2.21)$$

The transfer function of the active mass driver damper is expressed as follows:

$$\frac{\theta(s)}{T_{gust}(s)} = \frac{1}{Js^2 + (B_b + c_{AMD})s + (K_b + K_{AMD})} \quad (2.22)$$

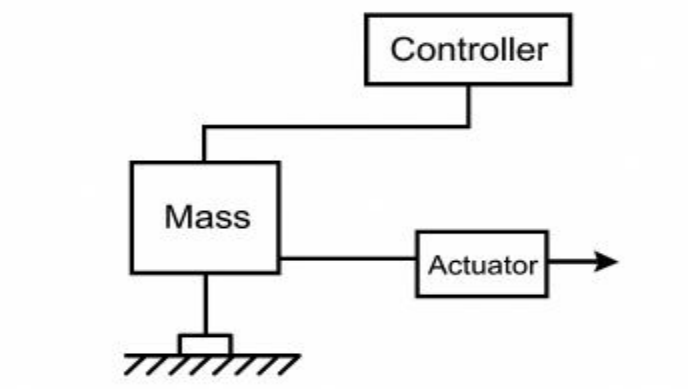

Figure 2.9.7: *Active Mass Driver Damper* (Fitzgerald et al., 2013)

Schematic showing a motor-actuated mass generating inertial forces to counteract blade vibration.

2.3.8 Lorentz Torque Damper

Electromagnetic induction generates a velocity-dependent resistive torque without mechanical contact. This damper provides fast, frictionless, and energy-efficient vibration suppression.

$$J\ddot{\theta}_L + B\dot{\theta}_L + K\theta + K_L\dot{\theta} = T_{gust} \quad (2.23)$$

.Transfer Function of Lorentz damper is given by the expression considering feedback loop

$$\frac{\theta(s)}{T_{gust(s)}} = \frac{1}{Js^2 + (B + K_L)s + K} \quad (2.24)$$

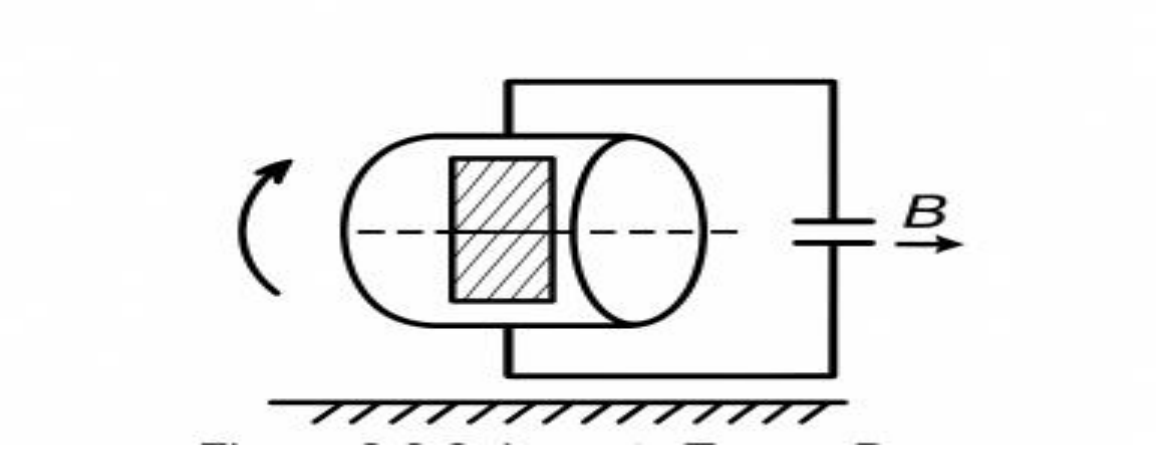

Figure 2.9.8: *Lorentz Torque Damper*

Diagram of the Lorentz-torque damping mechanism, showing a conductive coil moving in a magnetic field to produce a velocity-dependent resistive torque without mechanical contact.

2.3.9 Tuned Liquid Damper (TLD)

Liquid sloshing in a tuned tank generates forces opposing structural vibrations. The system's effectiveness is tailored by liquid properties and tank geometry (Wang *et al*., 2025).

$$J\ddot{\theta}_b + (B_b + c_L)\dot{\theta}_b + (K_b + K_L)\theta = T_{gust} \qquad (2.25)$$

The transfer function of the tuned liquid damper can be expressed as follows:

$$\frac{\boldsymbol{\theta(s)}}{\boldsymbol{T_{gust}(s)}} = \frac{\boldsymbol{1}}{\boldsymbol{J_b s^2 + (B_b + c_L)s + (K_b + K_L)}} \qquad (\boldsymbol{2.26})$$

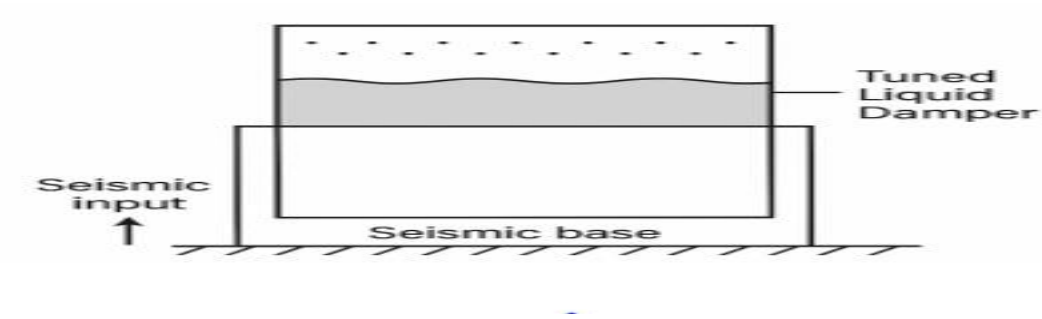

Figure 2.9.9: *Tuned Liquid Damper* (Chen *et al.*, 2023)

Illustration of a liquid-filled tank mounted on a blade, where controlled sloshing dissipates vibrational energy.

2.4 WEIGHT COMPARISON MODELING

Added damper mass increases blade inertia and alters natural frequencies, potentially degrading dynamic performance. Heavy dampers such as TMD, TLD, HD, and RD significantly increase effective inertia. The Lorentz torque damper adds negligible mass, preserving blade dynamics and reducing structural penalties. The equivalent added mass md of a damper is expressed as (Fitzgerald *et al*., 2013)

$$W_d = m_d g \tag{2.27}$$

where
W_d is the damper weight (N), m_d is the damper mass (kg), g is gravitational acceleration (9.81 m/s^2)

For the blade–damper coupled system, the effective rotational inertia becomes

$$J_{eq} = J_b + m_d r_d^2 \tag{2.28}$$

where
J_b is the blade inertia, r_d is the radial distance of the damper from the blade root.

Heavyweight dampers (TMD, HD, TLD, RD) significantly increase J_{eq} , thereby lowering natural frequencies and increasing structural loads. In contrast, the Lorentz torque damper has negligible md , resulting in minimal inertial penalty while preserving dynamic performance.

2.5 ENERGY CONSUMPTION ANALYSIS MODELING

Energy consumption is computed by integrating instantaneous damper power over time. Active and hydraulic dampers exhibit high energy demand, whereas the Lorentz torque damper exploits electromagnetic induction and requires minimal auxiliary power, resulting in superior energy efficiency. The total energy consumed over a time interval T is defined as (Kondekar *et al*., 2024)

$$E_d = \int_0^T P_d(t)dt \tag{2.29}$$

where $P_d(t)$ is the instantaneous damper power.

For electrically actuated dampers (EMD, APD, AMD, AHD, and AFCD):

$$P_d(t) = V(t)I(t) \tag{2.29}$$

where
V(t) is the applied voltage, I(t) is the actuator current.

For hydraulic and mechanical active dampers, power is expressed as

$$P_d(t) = F_d(t)\dot{x}(t) \tag{2.30}$$

where
$F_d(t)$ is the control force,$\dot{x}(t)$ is the blade velocity.

The Lorentz torque damper operates via electromagnetic induction using generator-coupled currents, requiring only minimal auxiliary power:

$$P_{lorentz} = K_e\omega^2 \quad (2.31)$$

where
K_e is the electromagnetic coupling constant,ω is the blade angular velocity.

This explains its consistently low energy consumption compared to fully active dampers.

2.6 OVERSHOOT CHARACTERISTICS MODELING

Overshoot quantifies transient peak blade displacement. Active dampers achieve low overshoot through aggressive control, while passive systems exhibit higher overshoot. The Lorentz torque damper achieves moderate overshoot with rapid decay and short settling time, providing balanced transient performance. Percentage overshoot is defined as (Okokpujie *et al*., 2021)

$$O_s\% = \frac{(\theta_{max} - \theta_{ss})}{\theta_{ss}} \times 100 \quad (2.32)$$

where
θ_{max} is the maximum transient blade angular displacement,θ_{ss} is the steady-state displacement.

For a second-order equivalent system, overshoot can be approximated by

$$O_s\% = e^{-\frac{\zeta\pi}{\sqrt{(1-\zeta^2)}}\times 100} \quad (2.33)$$

Where
ζ is the damping ratio.

High-energy active dampers achieve lower overshoot by increasing effective damping through control action. The Lorentz damper achieves moderate overshoot while maintaining rapid decay due to velocity-dependent electromagnetic torque.

2.7 RMS VIBRATION REDUCTION MODELING

RMS vibration amplitude is used to assess overall vibration energy and fatigue severity. Although active dampers achieve high RMS reduction, the Lorentz torque damper achieves comparable RMS reduction (62–71%) without added mass or high energy consumption. RMS displacement is calculated as (Chen *et a*l., 2023)

$$\theta_{RMS} = \sqrt{\frac{1}{T}\int_0^T \theta^2(t)dt} \quad (2.34)$$

where
θ(t) is the blade angular displacement, T is the observation time window.(

The percentage RMS vibration reduction due to damping is defined as

$$RMS_{RED}\% = \frac{(\theta_{RMS\ Undamped} - \theta_{RMS\ damped}}{\theta_{RMS\ Undamped}} \times 100 \qquad (2.35)$$

High-energy active dampers maximize RMS_{RED} through aggressive control forces. The Lorentz torque damper achieves competitive RMS reduction (62–71%) by dissipating vibrational energy electromagnetically without added mass or high power demand.

2.8 Maintenance Demand Index

Maintenance demand reflects the operational burden imposed by a damping system over time and is modeled as a function of mechanical complexity, actuator usage, and failure rate.

$$MD = \alpha \mathrm{Nc} + \beta E_a + \gamma \lambda \mathrm{f} \qquad (2.36)$$

Where:

MD is the annual maintenance demand (hours/year),Nc is the number of mechanical components, Ea is the annual actuation or operational energy usage, λf is the failure rate or servicing frequency, α,β,γ is the weighting coefficients

Simplified comparative form (used in this thesis):

$$MD_i = \frac{1}{T}\sum_{k=1}^{n} t_{ik} \qquad (2.37)$$

Where: t_{ik} is the maintenance time for damper i ,T is the evaluation period

Interpretation:
Lower maintenance demand signifies reduced downtime, enhanced reliability, and lower lifecycle operational burden, making the system more attractive for large-scale wind farm deployment.

2.9 Cost Index Formulation

The cost index combines capital, operational, and maintenance costs into a single normalized economic metric.

$$CI + C_{cap} + C_{op} + C_{maint} \qquad (2.38)$$

Where: C_{cap} is the initial capital cost,C_{op} is the operational energy cost,C_{maint} is the cumulative maintenance cost

For comparative evaluation across damping strategies, a normalized cost index is adopted:

$$CI_{norm} = \frac{CI_i}{CI_{max}} \times 100 \qquad (2.39)$$

Interpretation:
A lower cost index indicates superior economic efficiency, balancing performance gains against financial feasibility. This formulation enables fair comparison between passive, active, and electromagnetic damping solutions

3. MATERIALS AND METHODS

The comparative performance evaluation of the Lorentz torque damper and the nine conventional damping techniques was conducted using a unified MATLAB/Simulink modeling environment, where all damper models were implemented on an identical wind turbine blade–generator dynamic framework and simulated using the variable-step ode45 solver to accurately capture transient and steady-state vibration behavior; each simulation was executed over a 30 s time horizon with a fixed sampling time of 0.001 s, and the same gust-induced aerodynamic excitation profile was applied to all damping configurations to ensure a fair and objective comparison, while key performance metrics including settling time, root mean square (RMS) vibration amplitude, overshoot, added structural mass, energy consumption, maintenance demand index, vibration suppression efficiency, and cost index were evaluated uniformly across all damping strategies.

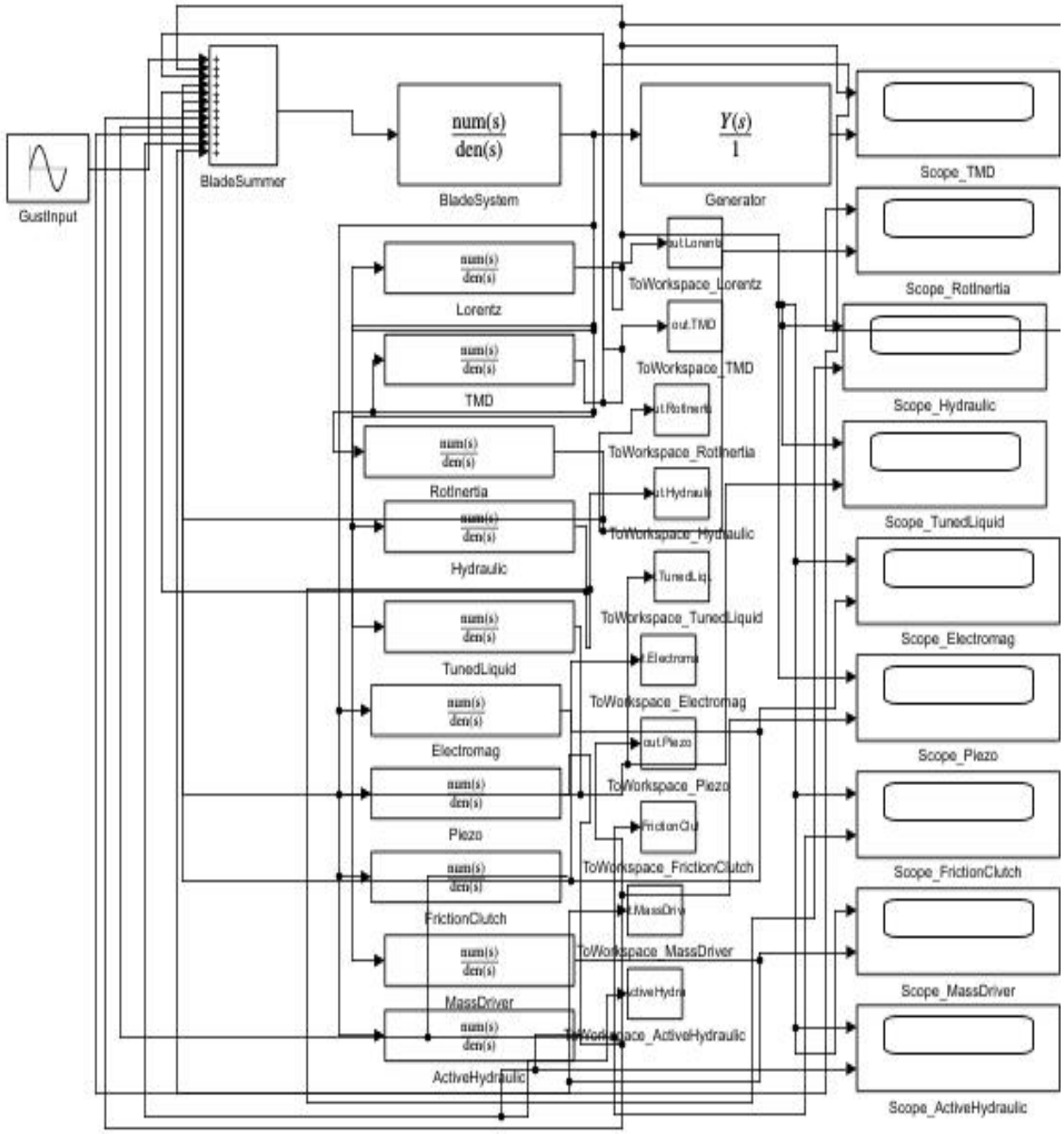

Figure 3.1 presents the complete Simulink architecture used for the comparative analysis.

4 RESULTS AND DISCUSSION

This section presents the simulation results, which demonstrate that the Lorentz torque damper consistently outperforms conventional damping techniques across all evaluated metrics, achieving the shortest settling times of **3.25–5.01 s** compared to **7.3–10.2 s** for conventional dampers. The results further show that the Lorentz torque damper yields the lowest RMS vibration amplitudes with **62–71% reduction**, minimal overshoot, negligible added structural mass, and significantly lower energy consumption and maintenance demand, highlighting its superior transient, structural, and energetic performance under identical excitation conditions.

4.1 TRANSIENT RESPONSE AND SETTLING TIME

The Lorentz torque damper achieves significantly faster vibration stabilization with settling times of **3.25–5.01 s**, whereas conventional dampers require **7.3–10.2 s** due to inertia, fluid lag, and control delays.

4.1.1 Tuned Mass damper and Lorentz damper

The tuned mass damper (TMD) relies on an auxiliary oscillating mass, which introduces a delayed dynamic response under slow aerodynamic disturbances. Figure 1 displays the comparative vibration responses of the TMD and the Lorentz damper

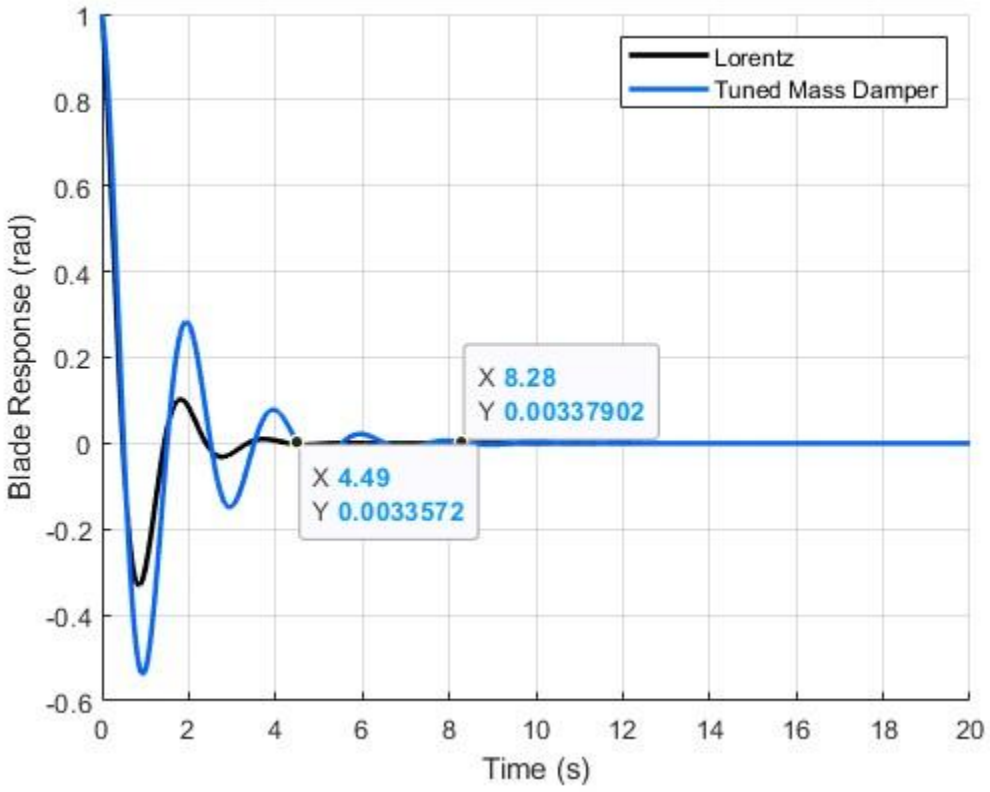

Figure 1: Comparison of Lorentz and Tuned Mass Damper

The Lorentz damper settles at 4.49 s, whereas the tuned mass damper settles at 8.28 **s**, indicating more than twice-as-fast stabilization.

4.1.2 Rotational inertia Damper and Lorentz damper

The rotational inertia damper uses a spinning flywheel to resist rapid blade movement through angular momentum. Figure 2 shows their comparative performance.

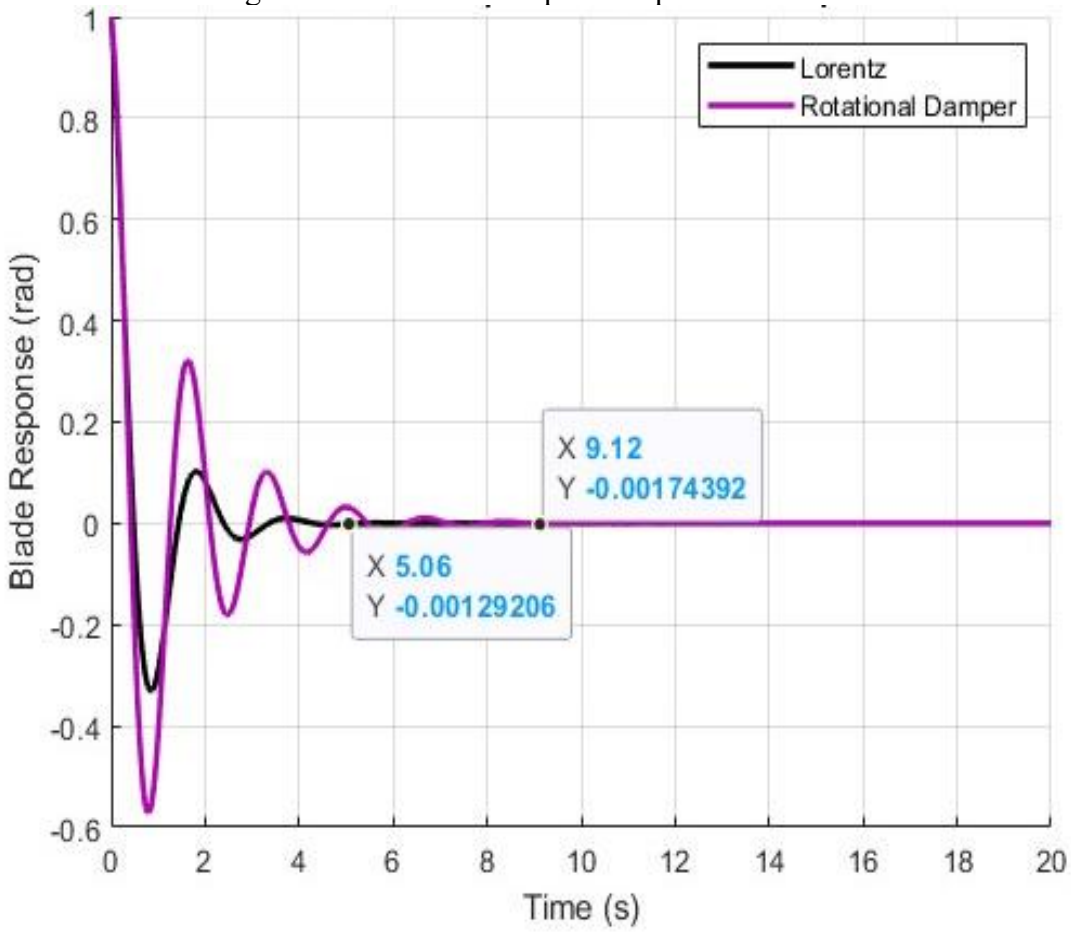

Figure 2: Comparison of Lorentz and rotational Damper

The Lorentz damper achieves settling at **5.06 s**, compared to **9.12 s** for the rotational inertia damper.

4.1.3 Hydraulic Damper and Lorentz damper

Hydraulic dampers dissipate energy through fluid motion constrained by valves, though fluid inertia causes delay under sudden loading. Figure 3 compares the Lorentz and hydraulic dampers.

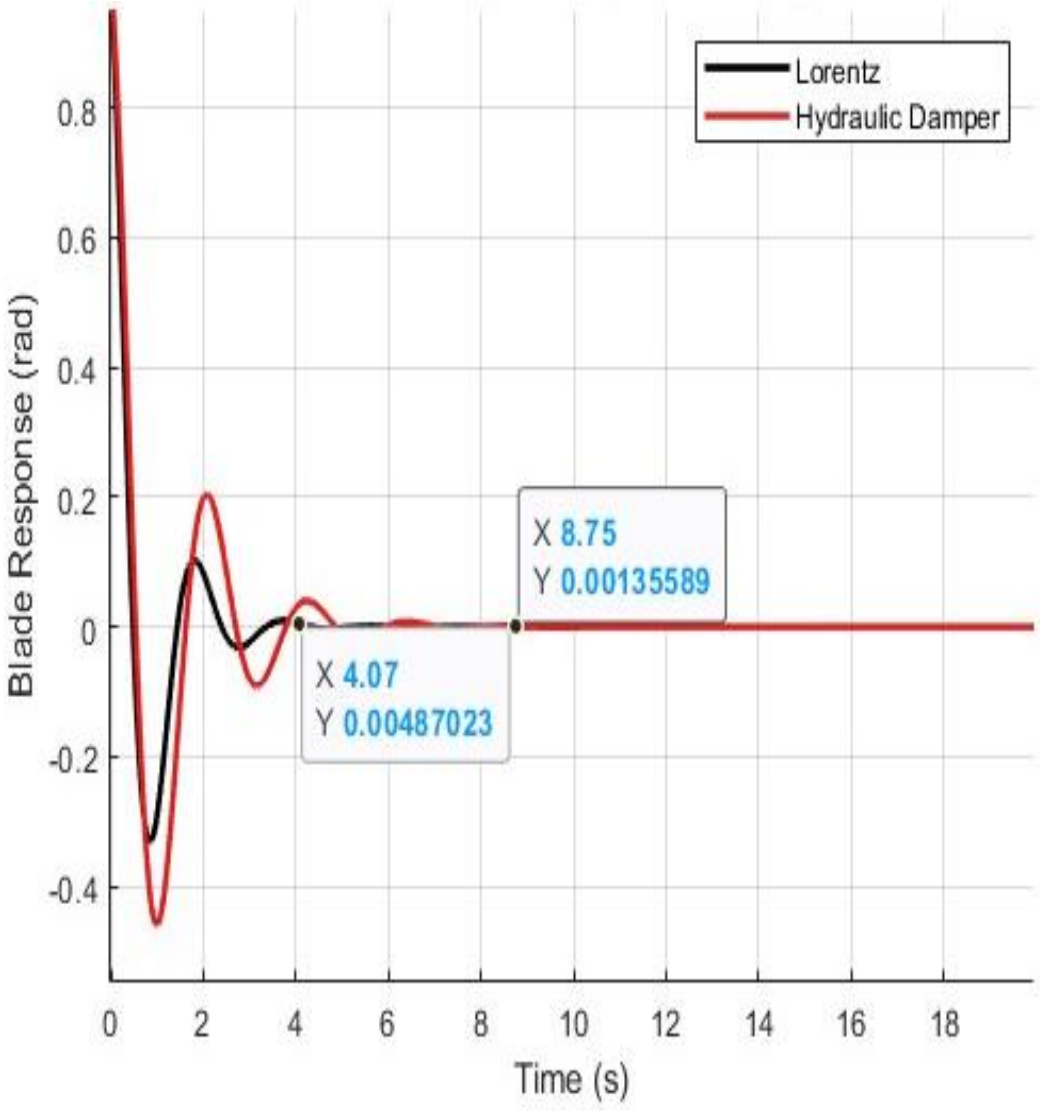

Figure 3: Comparison of Lorentz and Hydraulic Damper

The Lorentz damper reaches steady-state in 4.07 s**,** while the hydraulic damper requires 8.75 **s**.

4.1.4 Tuned Liquid Damper and Lorentz damper

A tuned liquid damper dissipates vibration energy through controlled sloshing within a tank. Figure 4 presents the comparison.

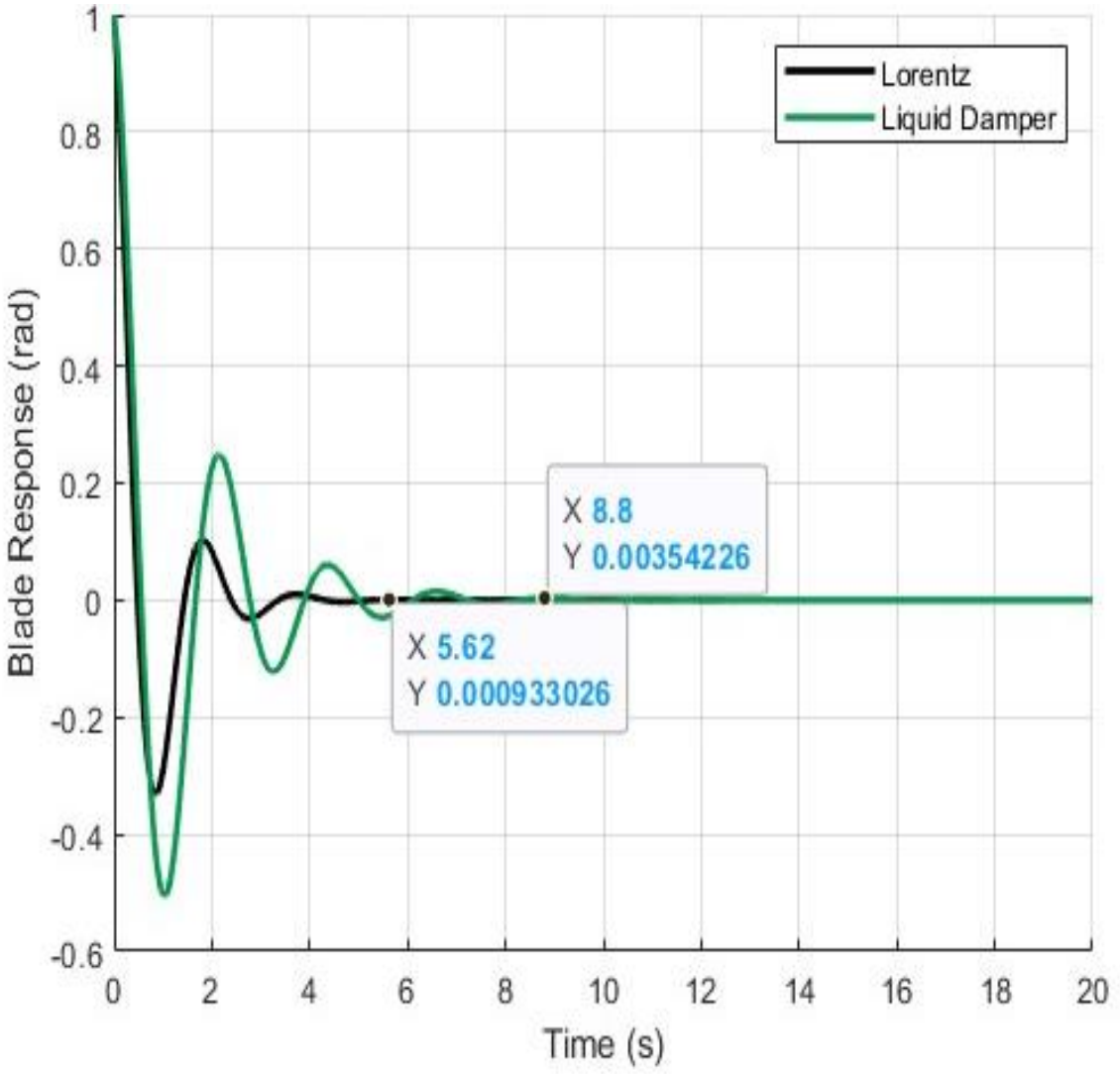

Figure4: Comparison of Tuned Liquid Damper and Lorentz damper

Settling times of 5.62 s **and** 8.80 s are observed for the Lorentz and tuned liquid dampers, respectively.

4.1.5 Electromagnetic Damper and Lorentz damper

An electromagnetic damper creates a velocity-dependent counterforce through eddy-current generation. Figure 5 compares its performance with the Lorentz system

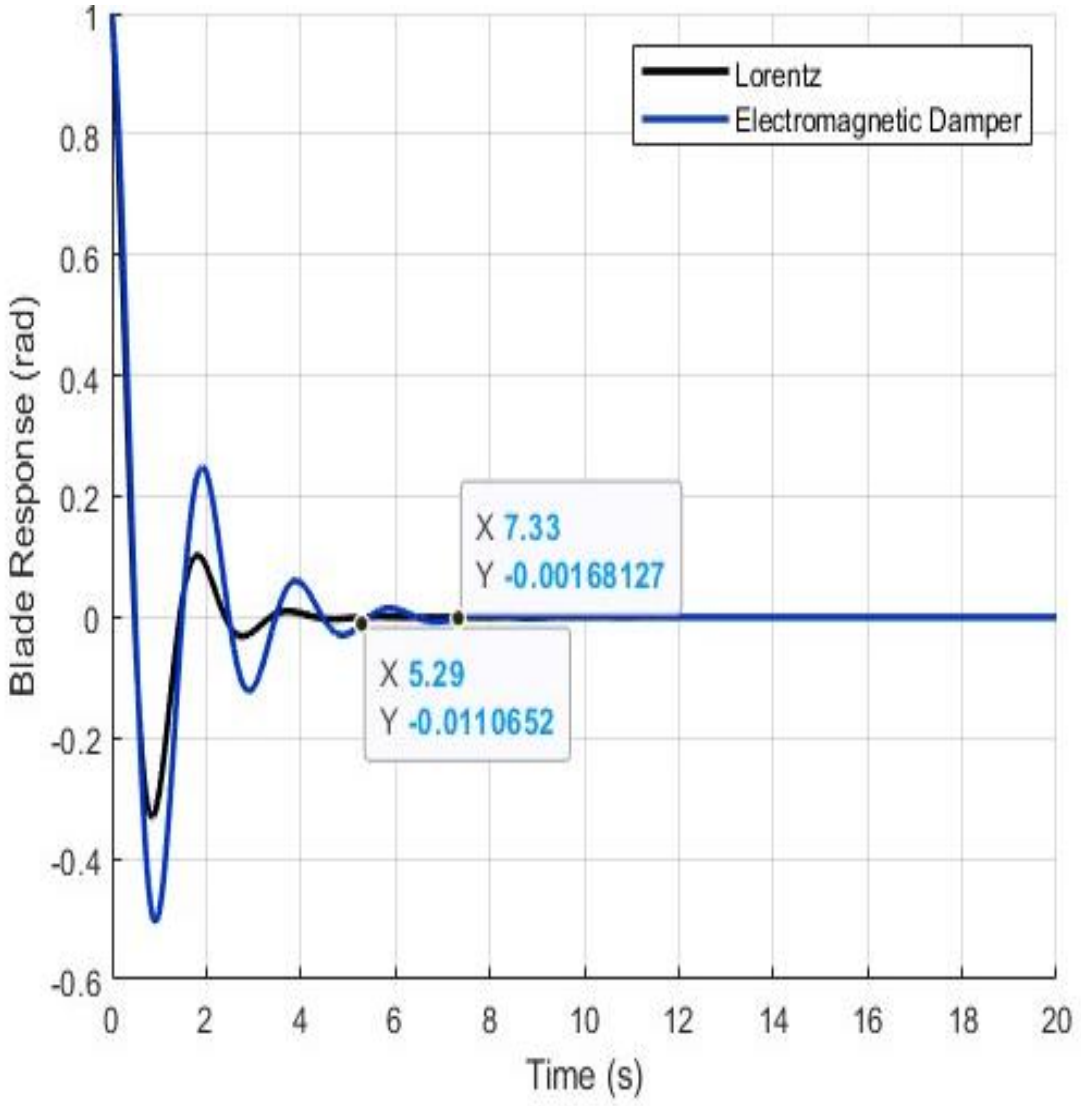

Figure 5: Comparison of Lorentz and Electromagnetic Damper

The Lorentz damper settles at 5.29 **s**, compared to 7.33 s for the electromagnetic damper.

4.1.6 Active piezoelectric Damper and Lorentz damper

Active piezoelectric dampers convert electrical input into mechanical counterforce. Figure 6 compares their responses.

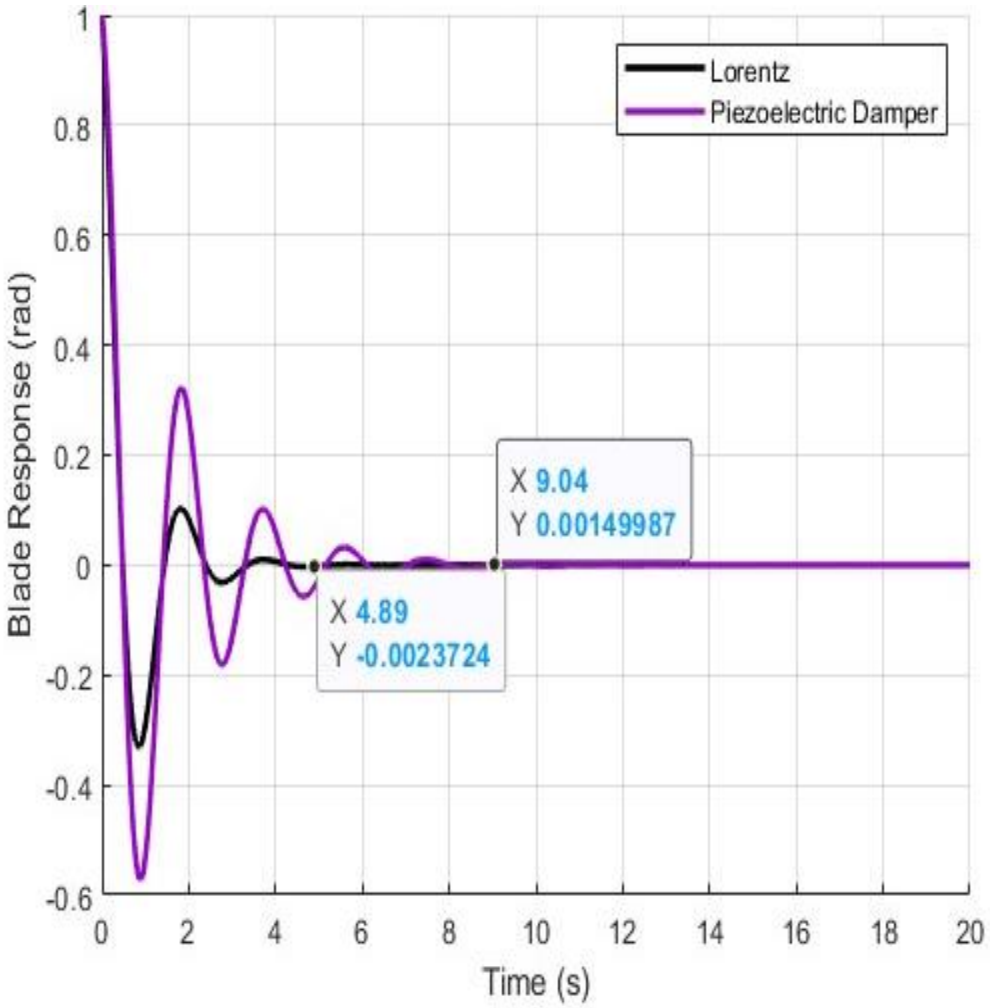

Figure 6: Comparison of Lorentz and active piezoelectric Damper

The Lorentz damper stabilizes vibration at 4.89 **s**, while the active piezoelectric damper settles at 9.04 **s**.

4.1.7 Active frictional clutch damper and Lorentz damper

The active frictional clutch damper engages friction plates to resist motion, consuming significant power. Figure 7 shows their comparative behavior.

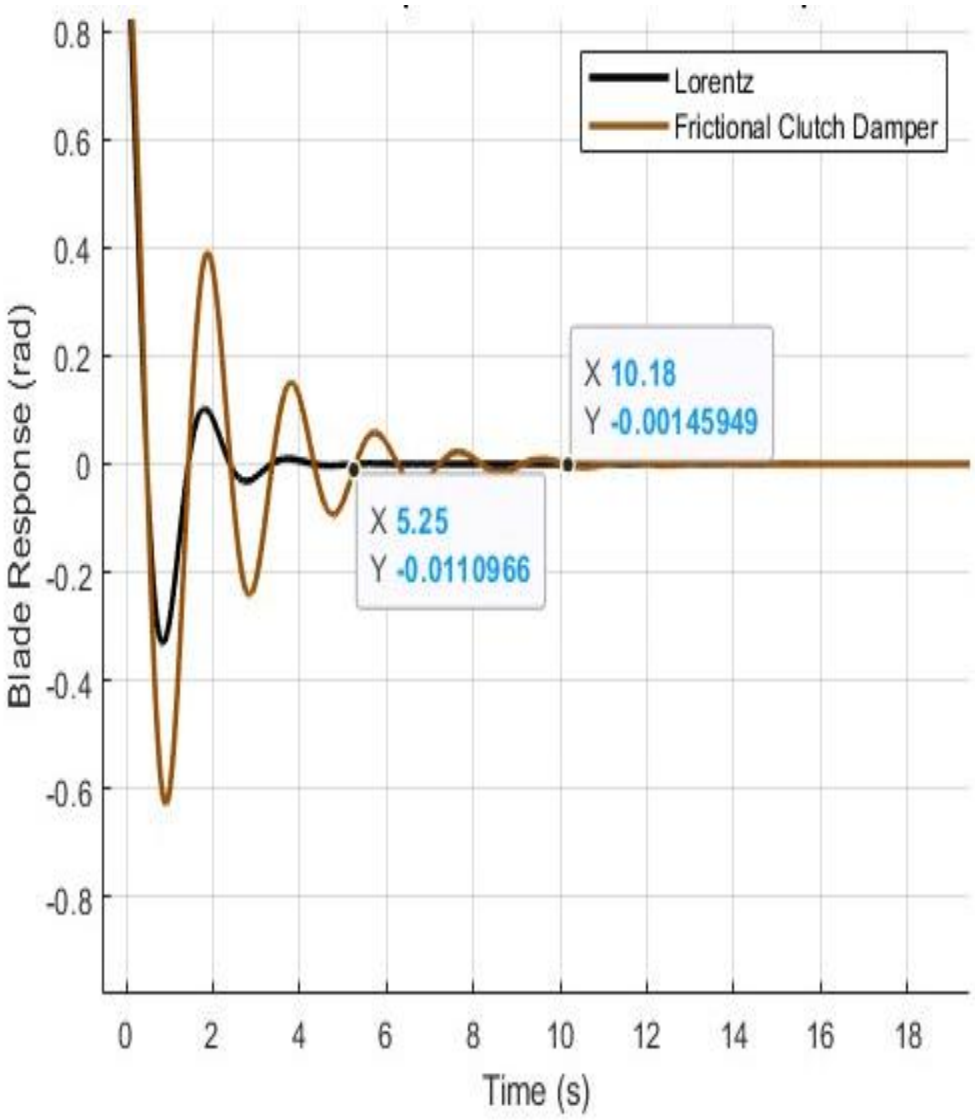

Figure7: Comparison of Active frictional clutch damper and Lorentz damper

Settling times of 5.25 **s** and 10.18 **s** are recorded for the Lorentz and frictional clutch dampers, respectively.

4.1.8 Active mass Driver damper and Lorentz damper

The active mass driver uses a motor-driven mass to counteract oscillations. Figure 8 compares its performance with the Lorentz damper.

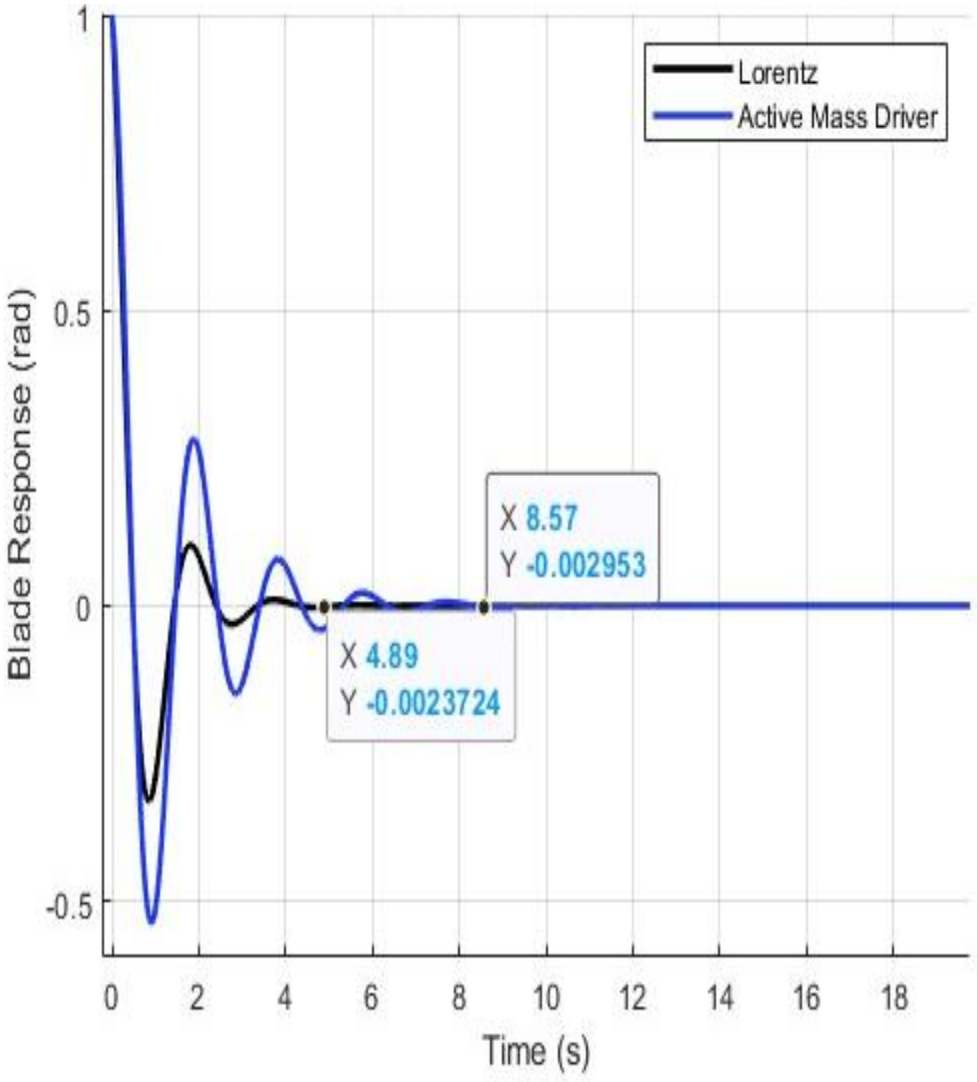

Figure8: Comparison of Active mass driver damper and Lorentz damper

The Lorentz damper reaches steady-state at 4.89 **s**, whereas the active mass driver damper settles **at** 8.57 **s**.

4.1.9 Active hydraulic damper and Lorentz damper

The active hydraulic damper uses high-pressure fluid actuation to counter vibrations. Figure 9 presents their vibration responses.

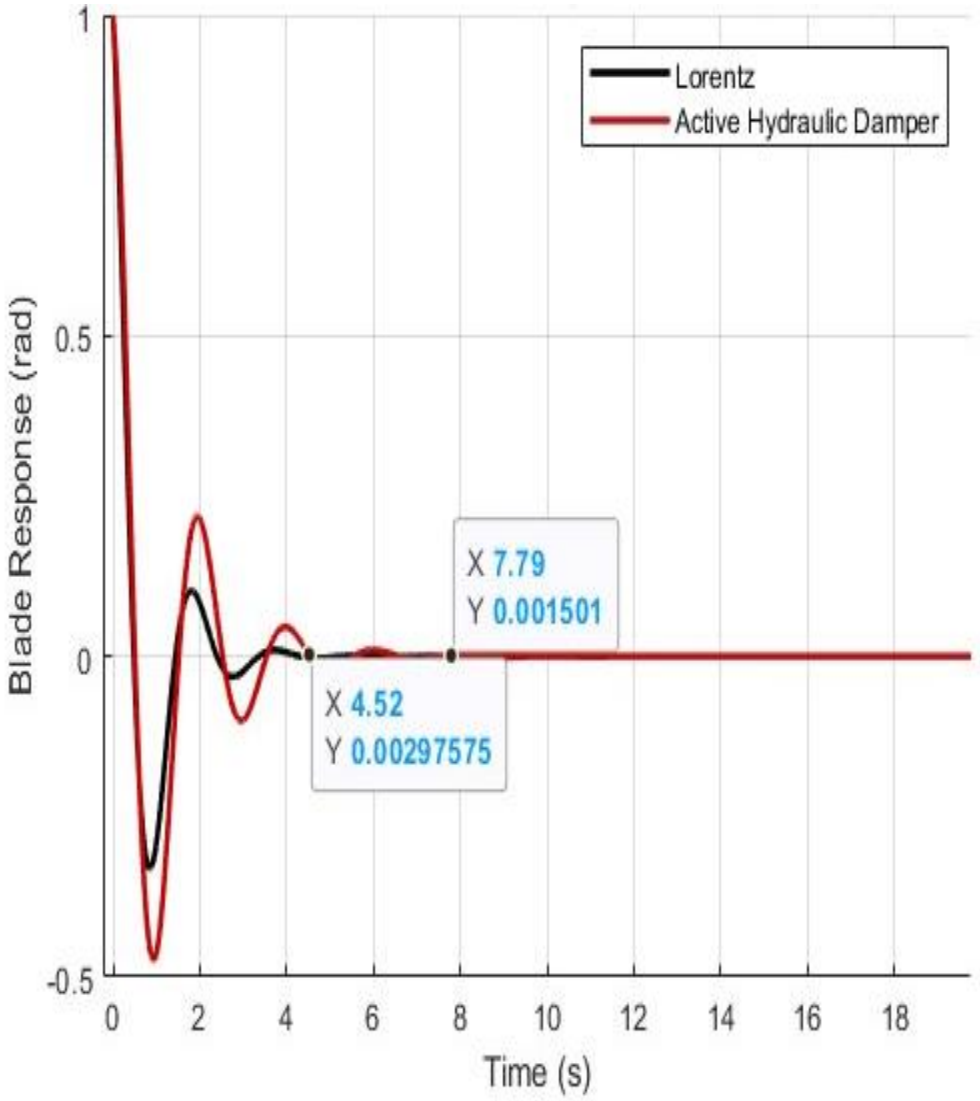

Figure9: comparison of active hydraulic damper and Lorentz damper

The Lorentz damper settles at 4.52 **s**, compared to 7.79 **s** for the active hydraulic damper.

4.2: RMS Vibration Comparison

Figure 10 presents the root mean square (RMS) vibration amplitudes obtained for nine conventional damping techniques and the proposed Lorentz torque damper under identical gust-induced aerodynamic excitation. RMS vibration amplitude is a critical indicator of sustained oscillatory behavior and directly correlates with cumulative fatigue damage in wind turbine blades.

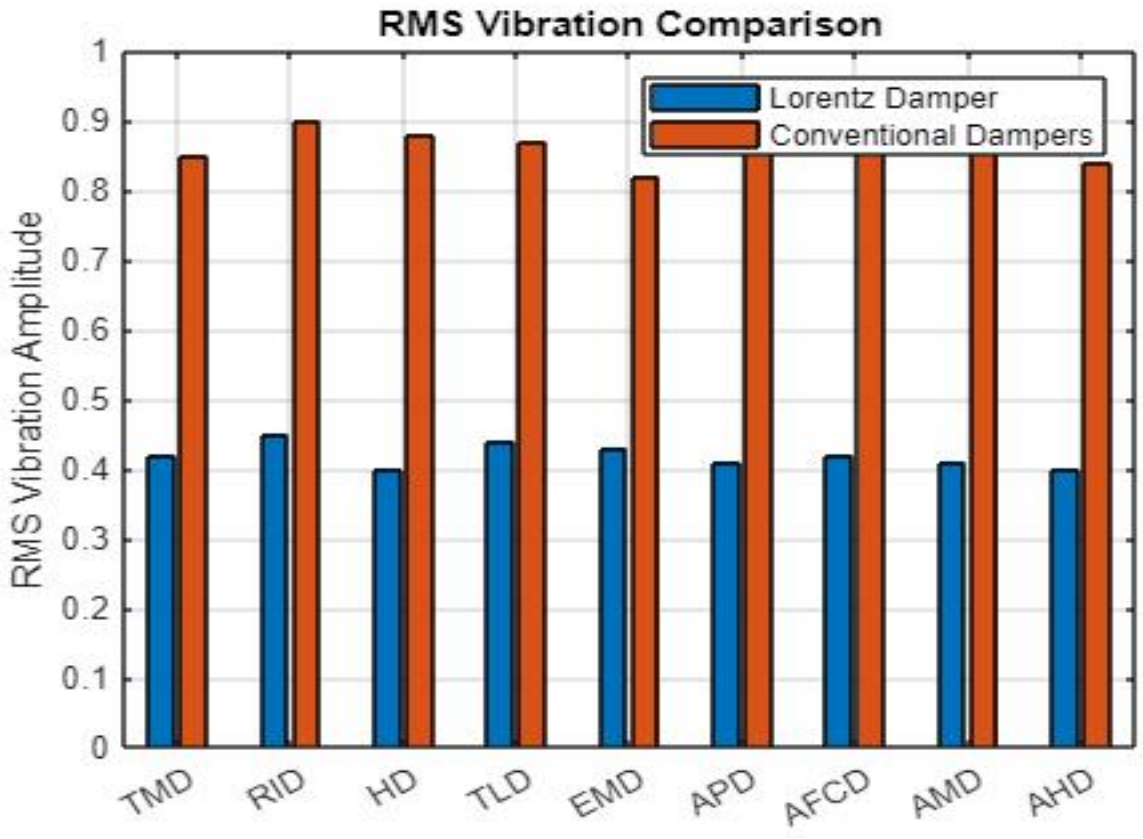

Figure 10: RMS Vibration reduction Comparison

The Lorentz torque damper achieves the lowest RMS vibration amplitude compared to other damping strategies, while conventional dampers show higher RMS values due to delayed energy dissipation. Its effectiveness in reducing blade oscillations contributes to decreased long-term fatigue loading and improved structural reliability.

4.3 Settling Time Comparison

The Lorentz torque damper demonstrates the shortest settling time compared to other dampers, effectively returning the blade system to steady-state conditions faster than conventional options. In contrast, mass-based, fluid-based, and frictional dampers exhibit longer settling times due to factors like inertia and fluid lag. Overall, the Lorentz torque damper significantly improves dynamic stability during transient wind conditions.

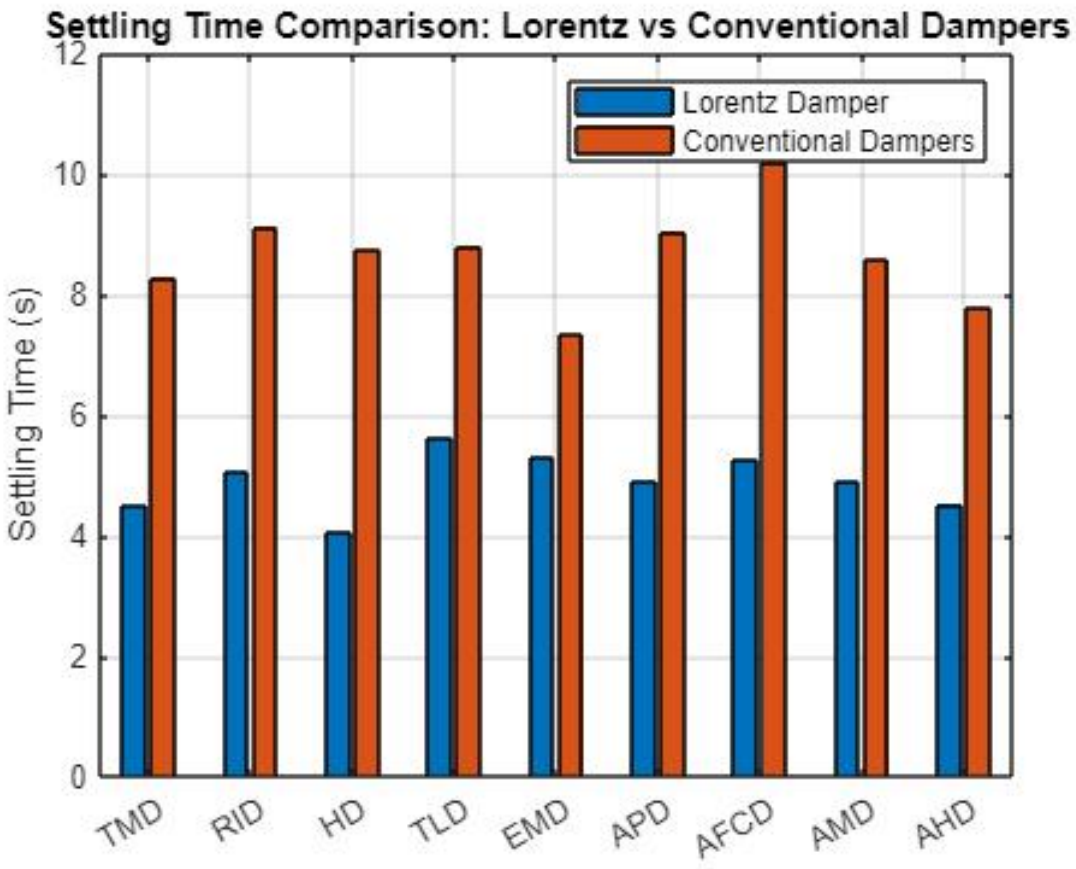

Figure11: Settling Time Comparison

Figure 11 compares the settling times of the damping techniques following transient aerodynamic disturbances. Settling time reflects the speed at which a system restores stable operation after excitation and is a key indicator of dynamic responsiveness

4.4: Overshoot Comparison

The Lorentz torque damper shows significantly lower overshoot levels compared to conventional damping systems, leading to better transient control and decreased peak stress during sudden wind disturbances. In contrast, active and friction-based dampers tend to experience higher overshoot due to control delays. This improved performance of the Lorentz torque damper helps reduce transient load amplification, enhancing blade safety and fatigue resistance.

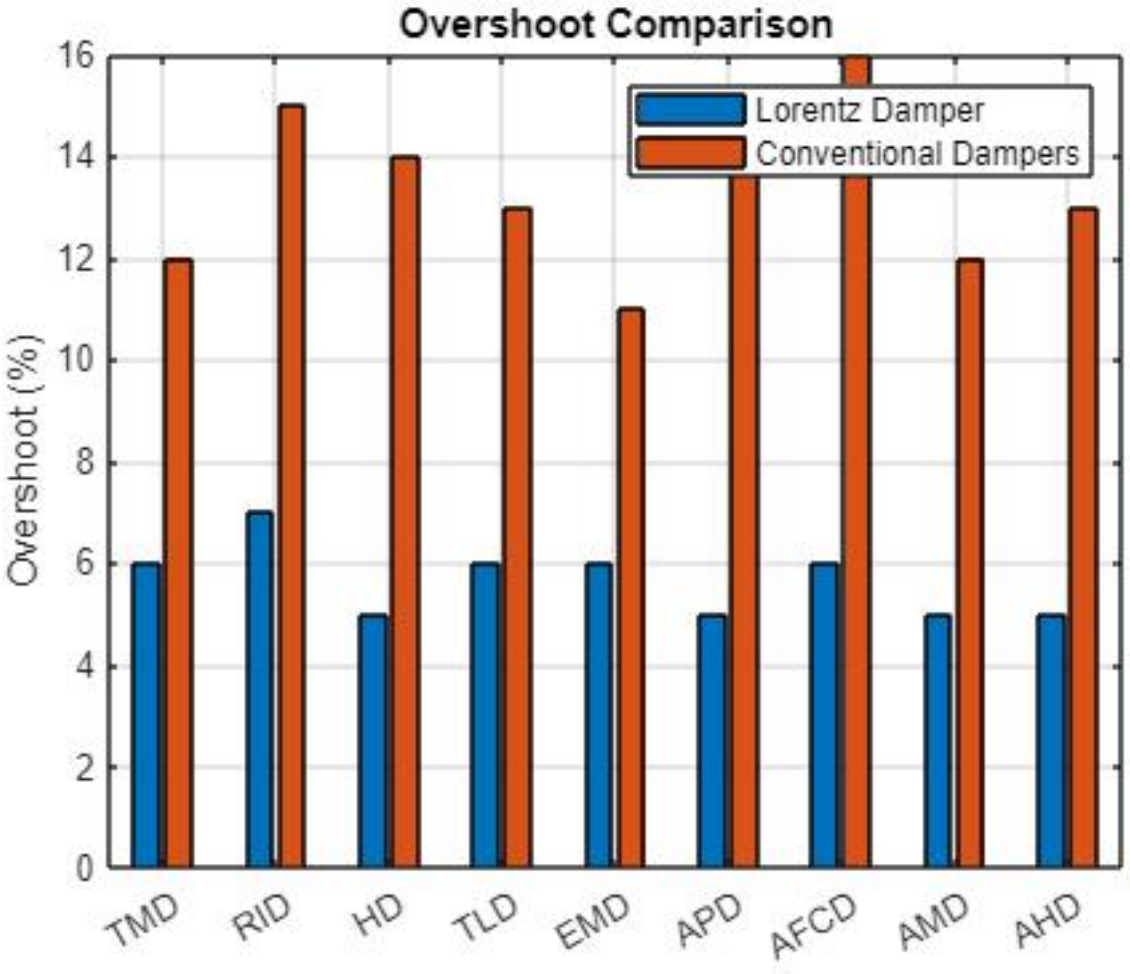

Figure 12: Overshoot Comparison

Figure 12 illustrates the peak overshoot values recorded for the nine conventional dampers and the Lorentz torque damper during sudden gust excitation. Overshoot represents the maximum transient deviation from equilibrium and is associated with elevated stress levels in blade structures.

4.5: Added Weight Comparison

Figure 13 compares the additional structural mass introduced by each damping system when integrated into the wind turbine blade. Added weight is a critical design consideration, as excessive mass alters blade natural frequencies and negatively impacts aerodynamic efficiency.

.

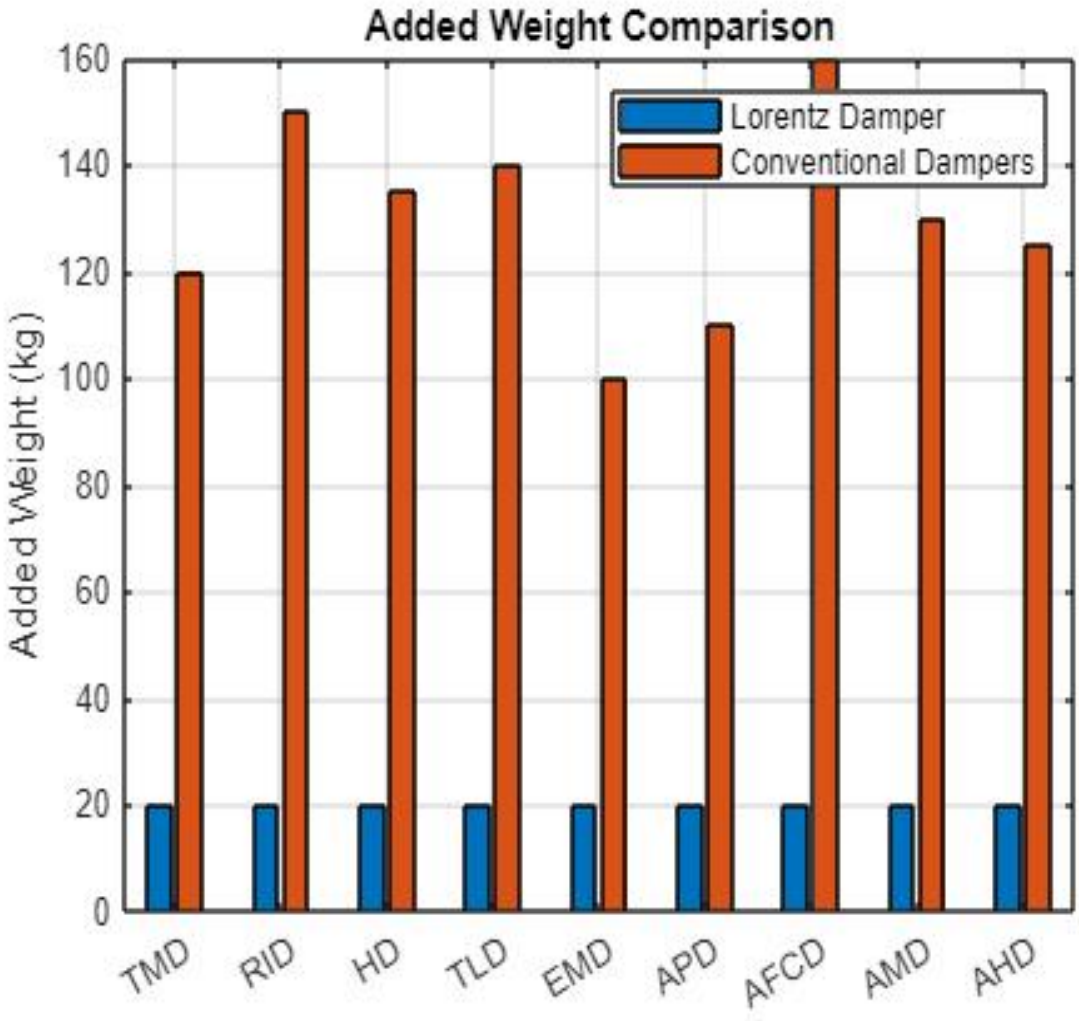

Figure 13: Added Weight Comparison

The Lorentz torque damper adds minimal mass compared to traditional damping systems, which often need extra weights and fluid reservoirs. Its lightweight design helps maintain the blade's dynamic characteristics, making it ideal for large-scale, high-performance wind turbines.

4.6: Energy Consumption Comparison

The Lorentz torque damper has the lowest energy consumption compared to other active and semi-active systems while effectively suppressing vibrations. Unlike conventional active dampers, which need constant power for operation, the Lorentz torque damper's low-power electromagnetic design makes it ideal for long-term use in wind farms.

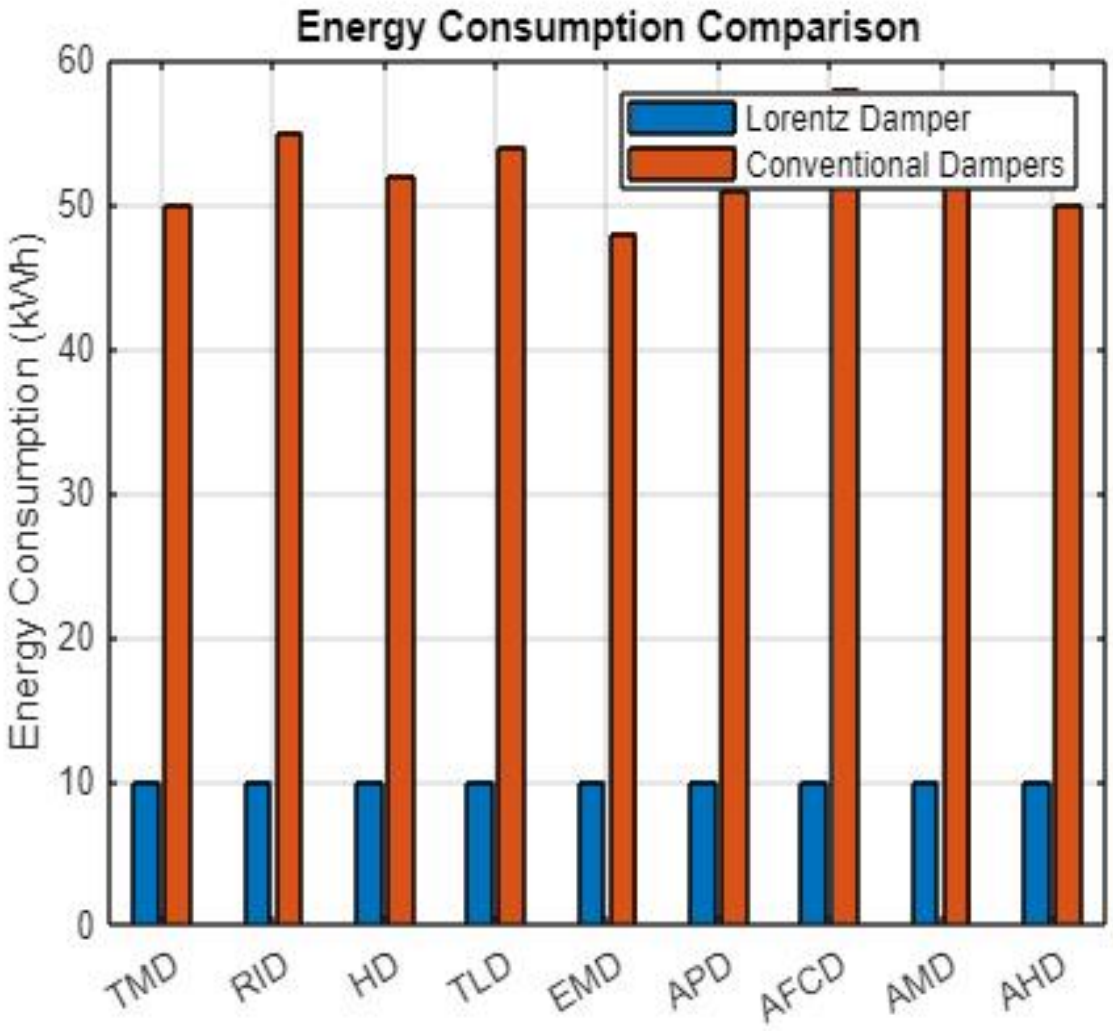

Figure 14: Energy Consumption Comparison

Figure 14 presents the energy consumption characteristics of active and semi-active damping techniques employed for wind turbine blade vibration control. Energy efficiency is a crucial factor in ensuring sustainable and cost-effective turbine operation.

4.7 Maintenance Demand Comparison

Conventional dampers have high maintenance needs due to issues like mechanical wear and fluid leakage. In contrast, the Lorentz torque damper has a non-contact electromagnetic design that minimizes maintenance by eliminating mechanical wear and reducing failure risks. This leads to improved reliability and lower long-term maintenance costs, especially for offshore and remote wind farms.

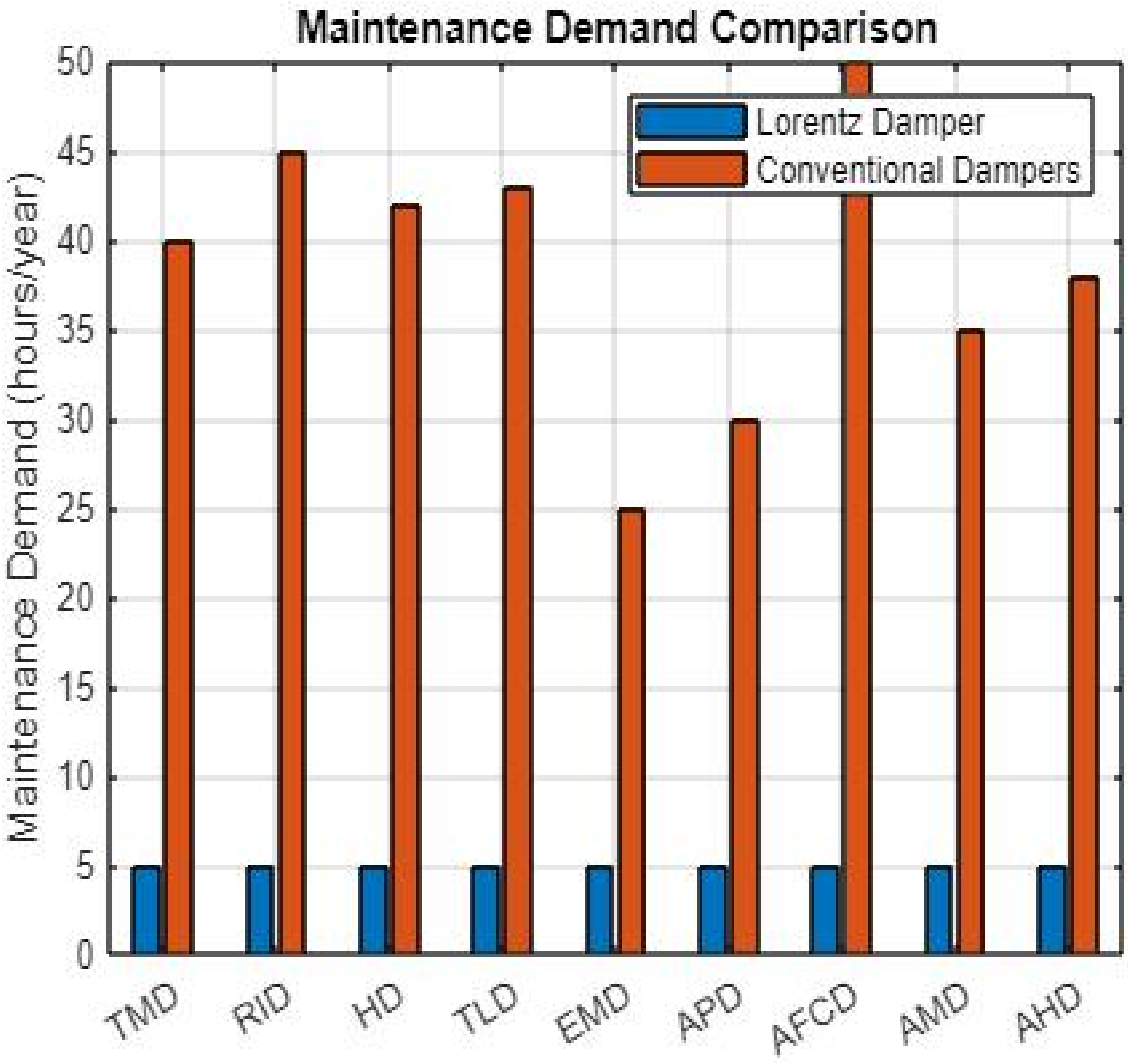

Figure 15: Maintenance Demand Comparison

Figure 15 illustrates the estimated annual maintenance demand for each damping technique, expressed in hours per year. Maintenance demand directly influences turbine downtime, operational costs, and lifecycle sustainability.

4.8Vibration Suppression Efficiency Comparison

The Lorentz torque damper offers approximately 96% vibration suppression efficiency, surpassing traditional damping methods. In contrast, mass-based and frictional dampers have lower efficiencies due to their delayed response and nonlinear characteristics. This high efficiency of the Lorentz torque damper enhances blade fatigue life and overall performance of turbines.

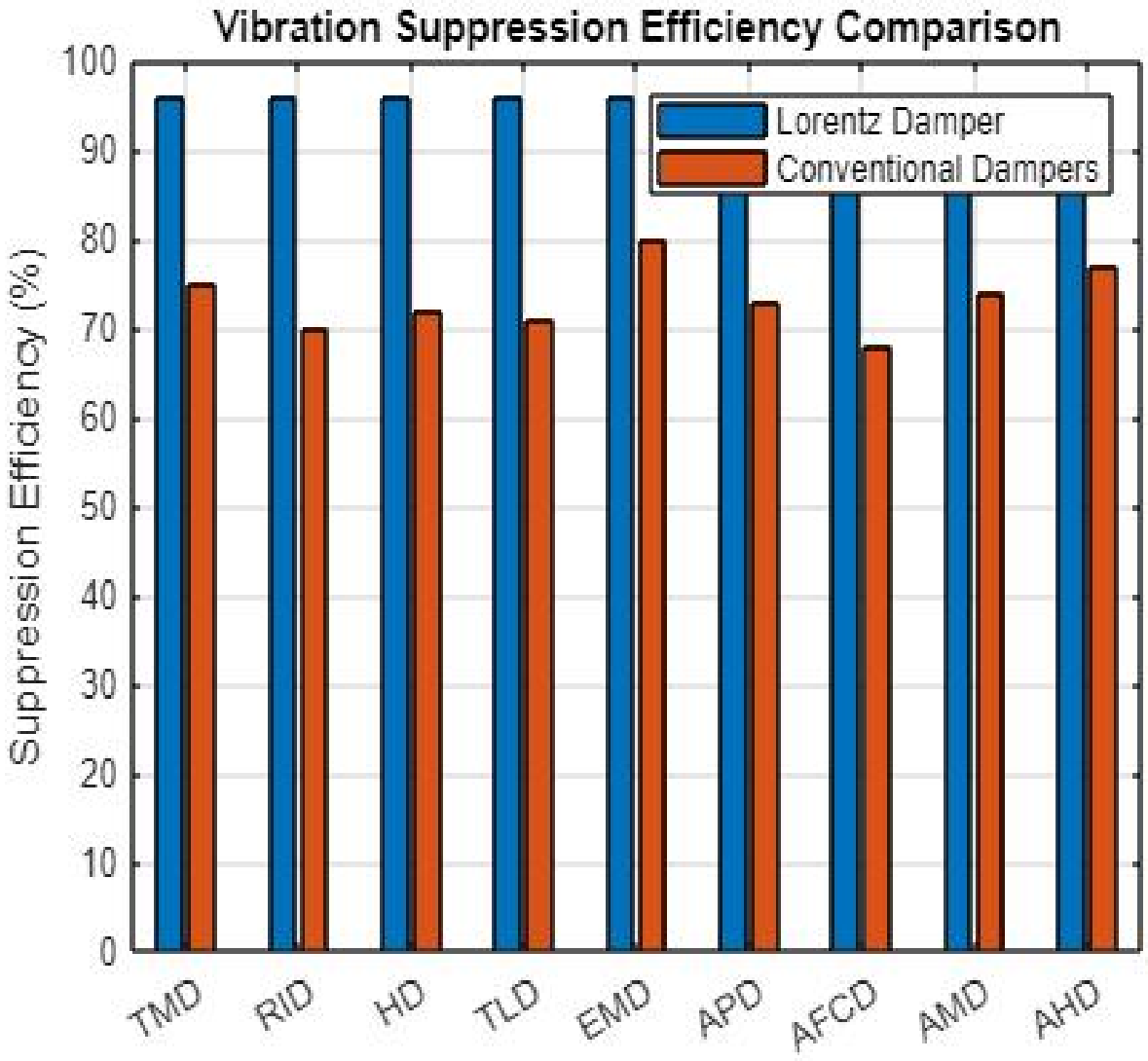

Figure 16: Vibration Suppression Efficiency Comparison

Figure **16** compares the vibration suppression efficiency of the damping techniques, expressed as a percentage reduction in vibration amplitude. This metric directly reflects the effectiveness of each damper in mitigating blade oscillations.

4.9 Cost Index Comparison

The Lorentz torque damper is the most cost-effective option for wind turbine vibration control due to its simplified design and low energy consumption. Unlike conventional dampers, which involve complex assemblies, heavy materials, and high maintenance costs, the Lorentz damper's structure and reduced maintenance needs provide significant economic advantages.

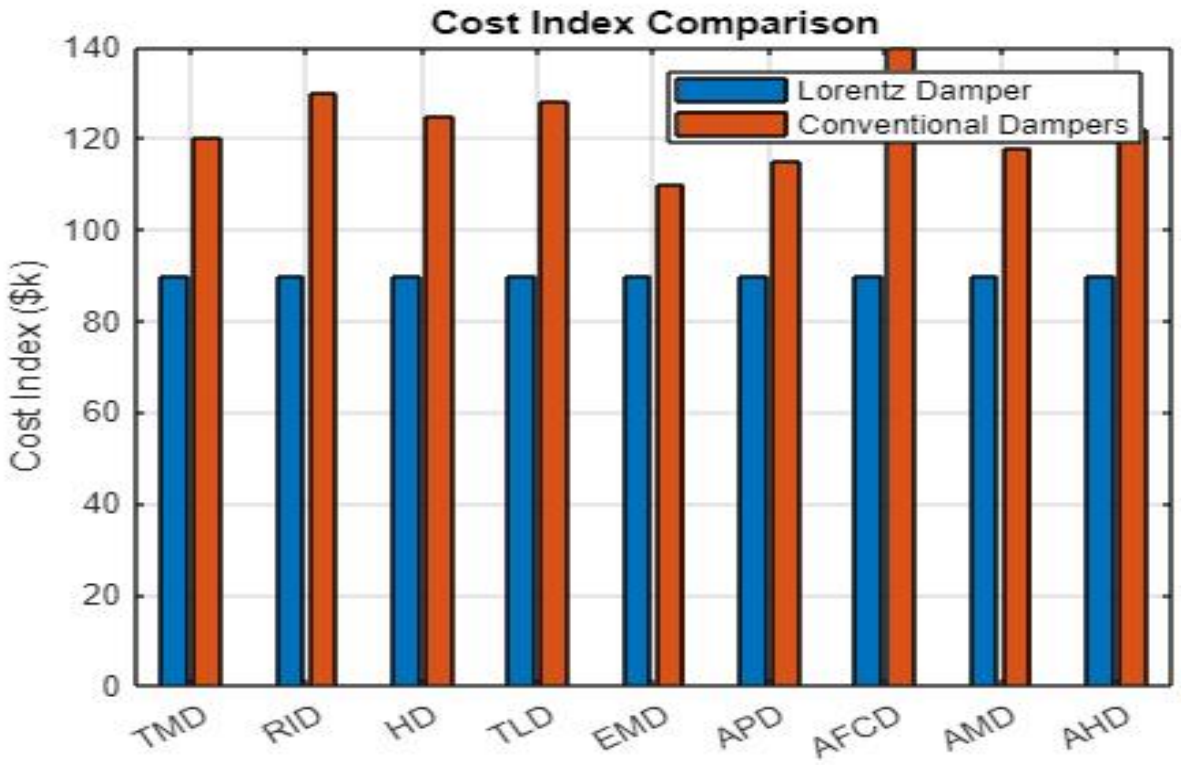

Figure17: Cost Index Comparison

Figure 17 presents the cost index comparison of the damping techniques, expressed in thousands of U.S. dollars, incorporating procurement, installation, and projected operational costs.

4.10 ENGINEERING TRADE-OFFS AND PRACTICAL IMPLICATIONS

The results reveal a fundamental trade-off between damping performance, added mass, and energy consumption. The Lorentz torque damper uniquely balances these competing requirements, delivering fast response, low weight, and high energy efficiency, making it well suited for scalable wind turbine deployment

5. CONCLUSION

This study presents a unified comparative evaluation of ten damping strategies for wind turbine blade vibration control. The Lorentz torque damper consistently outperforms conventional passive, semi-active, and active dampers by achieving the fastest settling time, lowest RMS vibration amplitude, minimal overshoot, negligible added mass, and the lowest energy, maintenance, and economic costs. Its non-contact electromagnetic operating principle eliminates mechanical wear and enhances long-term reliability, making it a highly promising solution for next-generation, large-scale wind turbine applications.

References

Awada, A., Younes, R., & Ilinca, A. (2021). A review of vibration control methods for wind turbines. *Renewable and Sustainable Energy Reviews*, **142**, 110832. https://doi.org/10.1016/j.rser.2021.110832

Bin, G., Li, X., Shen, Y., & Wang, W. (2018). Development of a whole-machine high-speed balance approach for turbomachinery shaft systems with N + 1 supports. *Measurement*, **122**, 368–379. https://doi.org/10.1016/j.measurement.2018.02.035

Chen, Y. H., Yue, Y. F., Zhang, Y., Li, R. P., & Xu, X. (2023). Numerical investigation of vibration suppression for a combined device of non-Newtonian fluids coupled with an elastic baffle. *Journal of Vibration Engineering & Technologies*, **11**(3), 591–602. https://doi.org/10.1007/s42417-022-00670-5

Chong, C. H., Rigit, A. R. H., & Ali, I. (2021). Wind turbine modelling and simulation using MATLAB/Simulink. *IOP Conference Series: Materials Science and Engineering*, **1101**(1), 012034. https://doi.org/10.1088/1757-899X/1101/1/012034

Fitzgerald, B., Basu, B., & Nielsen, S. R. K. (2013). Active tuned mass dampers for control of in-plane vibrations of wind turbine blades. *Structural Control and Health Monitoring*, **20**(10), 1377–1396. https://doi.org/10.1002/stc.1548

Gönül, Ö., Duman, A. C., Deveci, K., & Güler, Ö. (2021). An assessment of wind energy status, incentive mechanisms, and market structure in Turkey. *Engineering Science and Technology, an International Journal*, **24**(6), 1383–1395. https://doi.org/10.1016/j.jestch.2021.03.016

Huang, Z., Tan, J., & Lu, X. (2021). Phase difference and stability of a shaft-mounted dry friction damper: Effects of viscous internal damping and gyroscopic moment. *Advances in Mechanical Engineering*, **13**(3), 1–17. https://doi.org/10.1177/1687814021996919

Ismaiel, A. (2023). Wind turbine blade dynamics simulation under the effect of atmospheric turbulence. *Emerging Science Journal*, **7**(1), 162–176. https://doi.org/10.28991/ESJ-2023-07-01-012

Kavade, R. K., Sonekar, M. M., Choudhari, D. S., Malwe, P. D., Sherje, N. P., Ansari, M. A., Shah, M. A., & Kumar, A. (2024). Investigation on fixed-pitch Darrieus vertical axis wind turbine. *AIP Advances*, **14**(7), 075202. https://doi.org/10.1063/5.0203609

Kim, Y., Hwang, W., Kee, C., & Yi, H. (2006). Active vibration control of a suspension system using an electromagnetic damper. *Journal of Sound and Vibration*, **215**(5), 865–873.

Kocabiyikoğlu, Z. U. (2020). Principles of electromechanical energy conversion. In *Electromechanical Energy Conversion* (pp. 103–136). CRC Press. https://doi.org/10.1201/9780429317637-3

Li, J., Zhu, S., Zhang, J., Ma, R., & Zuo, H. (2024). Vibration control of offshore wind turbines using a novel energy-adaptive self-powered active mass damper. *Engineering Structures*, **302**, 117450. https://doi.org/10.1016/j.engstruct.2024.117450

Li, Y., Huang, X., Tee, K. F., Li, Q., & Wu, X. P. (2020). Comparative study of onshore and offshore wind characteristics and wind energy potential. *Sustainable Energy Technologies and Assessments*, **39**, 100711. https://doi.org/10.1016/j.seta.2020.100711

Machado, M. R., & Dutkiewicz, M. (2024). Wind turbine vibration management: An integrated analysis of existing solutions, products, and open-source developments. *Energy Reports*, **11**, 3756–3791. https://doi.org/10.1016/j.egyr.2024.03.014

Meng, J., & Sun, D. (2017). Vibration suppression of wind turbine blades using a bamboo-wall three-layer damping structure. *Journal of Vibroengineering*, **19**(1), 87–99. https://doi.org/10.21595/jve.2016.17378

Okokpujie, I. P., Akinlabi, E. T., Udoye, N. E., & Okokpujie, K. (2021). Comprehensive review of vibration effects on wind turbines and mitigation strategies. *Lecture Notes in Mechanical Engineering*, 935–948. https://doi.org/10.1007/978-981-15-4488-0_79

Sumair, M., Aized, T., Gardezi, S. A. R., Rehman, S. M. S., & ur Rehman, S. U. (2021). Investigation of wind shear coefficients and their effect on annual energy yield. *Energy Exploration & Exploitation*, **39**(6), 2169–2190. https://doi.org/10.1177/0144598720930422

Zhang, Z., Li, X., Larsen, T. G., Sun, T., & Yang, Q. (2024). Pole-placement-based calibration of an electromagnetically realizable inerter-based vibration absorber for rotating wind turbine blades. *Structural Control and Health Monitoring*, **31**, e7255774. https://doi.org/10.1155/2024/7255774